

Quantum Hall Effect at 40 kelvin: Evidence of Macroscopic Quantization in the Extreme Soft Limit

Timir Datta, Michael Bleiweiss, Anca Lungu and Ming Yin

Physics & Astronomy Dept., and the Nanocenter
University of South Carolina, Columbia, SC 29208, USA.

Zafar Iqbal
Chemistry Department
New Jersey Institute of Technology
Newark, NJ, USA.

Quantum Hall Effects ^{1,2} (QHE) are of two types, ^{3,4} the integer effect is a direct result of Landau level quantization of noninteracting electrons, and the fractional effect similar to superconductivity, is a macroscopic quantum phenomenon but arise from a new form of electronic condensation into a strongly correlated quantum liquid (QL). Usually QHE are observed in very high mobility, two-dimensional, electron (hole)-gas or (TDEG) systems typically under high magnetic fields (B) and at low temperatures (T), i.e., in the extreme quantum limit ($B/T > 1$). Quantum Hall effect is applied as calibration benchmark, international resistance standard, and a characterization technique for semiconductor heterostructures. Applications can be widespread if the devices and the operating conditions were more accessible. Here we report evidence of both fractional and integer quantum hall effects (2/3, 4/5, 1, etc) in a novel carbon structure, in a remarkably soft quantum limit of $T \sim 40K$.

As indicated above, the devices that contain the TDEG themselves are complex quantum well structures. The fabrication of these hetero-junctions is a marvel of modern semiconductor manufacturing. Not surprisingly the exploration for new simpler systems and understanding the nature of the quantum hall states under low magnetic fields⁹ are contemporary topics of research.

Our strategy to achieve the desired quantum properties has been by modifying the materials geometry and the mesoscale confirmation. Mesoscale shape¹⁰ and nontrivial atomic coordination¹¹⁻¹⁴ are known to enhance quantum-mechanical transport properties. The system of choice belongs to a new class of solids, replica opals, three-dimensional carbon replica opals (CRO) in particular. Introduced by Bogomolov et al¹⁵, these are structurally complimentary to artificial (porous) opals and have recently received a considerable attention as a new source of self-aggregated, nano-structured solids. The properties of these materials depend on the opal sphere size and preparation. They form optical cavities¹⁶ photonic bandgap crystals¹⁷ and superconductors¹⁸.

Our specimens were fabricated from silica opals, by a process of chemical vapor deposition (CVD) of carbon from propylene (C₃H₆) gas; carbon grows as surface layers on the silica spheres to form a closed packed stacking of mesoscopic “carbon-eggshells”. After the desired amount of carbon is deposited the silica spheres are removed by chemical etching. More details about deposition may be found in reference 16. The freestanding carbon regions are multiply connected¹⁹ and form a lattice of interconnected

percolating paths. The thickness of the carbon is uneven and depends on the (local) infiltration rate of the gas. For example no deposition takes place so thickness is zero and holes are left behind at places where the vapor penetration is obstructed, such as in the contact regions between the silica spheres.

The sphere diameter of the samples is about 250nm. A picture of a cleaved surface is shown in figure 1. The inset at the left corner is a color-enhanced image of the interior of two half shells. The one on the lower right is another view of the shell stacking. The arrows mark some of the foramens in the carbon shells.

For transport experiments the specimens were cut into small rectangular (2x4x5mm) blocks and gold or copper electrodes were attached in the standard four and six terminal geometry. Phase sensitive measurements were performed in first our laboratory at USC, for temperatures upto 40K and at low fields ($B < 3$ tesla) in an ultra-low noise, cryostat with a superconducting magnet. Through out a run T held constant, and B was varied in steps according to a preset program. Each measurement was taken with B held constant and the magnet in the “latch” mode. At the National High Magnetic Field Laboratory, (NHMFL) in Tallahassee, Florida, higher field ($B < 20$ T) experiments were performed while B was ramped up and down.

We observe that these samples were electrically non-metallic, i.e., resistance, $R(T)$, increases as temperature was reduced (figure 2). However, charge transport is not simply activated at low temperatures evidence for weak localization¹⁹ and carrier motion was via variable range hopping (VRH) between localized states were observed²⁰. The inset plot of figure 2 shows localization and VRH behavior.

With a magnetic field (B) applied along the z-axis and current flowing along x-axis both the longitudinal magneto response (R_{xx}) and that perpendicular to both current flow and B i.e., Hall voltage, V_{xy} (or R_{xy}) were measured simultaneously. As B was increased hall resistance followed the well-known signature of quantum hall effect - a unique step pattern. Correlated with the steps of V_{xy} , R_{xx} showed quantum-oscillations due to Subnikov-deHass (SdHass) effect. Figure 3 is a von Klitzing plot of the V_{xy} and R_{xx} isotherms at 38K. Even at this relatively elevated temperature Subnikov oscillations and hall plateaus were resolved with good synchrony between V_{xy} and the magneto-resistance.

It may be shown²¹ that a direct proportionality exists between the field B of the SdHaas minima and V_{xy} , or the corresponding resistance $R(v)_{xy}$ steps as follows,

$$B = (en_s)R_{xy} \quad \dots 1$$

Where, e is the unit of electric charge and n_s is the carrier density and n_s can be determined from a fit of the data to equation 1, and the values of the Landau-levels filling factor (v) corresponding to the plateaus in the hall curve are given by §:

$$(v)^{-1} = \left(\frac{e}{n_s h}\right)B \quad \dots 2$$

The hall plateaus in figure 3, were designated by the values of v as estimated from equation 2.

The Landau-levels that were particularly prominent, are the rational fraction filling factors $v = p/q$ (p, q are integers) $2/3$, $4/5$ and the integers 1 and 2 another high integer step with fill factor of 12 was also noticed. It may be useful to compare some literature values of field and temperature required for QHE in high mobility, samples; for

example in a 500Å wide modulation-doped GaAs/AlGaAs, heterostructure in 35 mK, the “2/3” state is observed at a little over 6 tesla²². In Bi_{2-x}Sn_xTe₃ the “2” state is recorded at 0.3 K and ~9 T²³. High filling factor states can be condensed at low magnetic fields, such as ~0.2 tesla for the “36” state, but at a temperature of 50mK²⁴. These are orders of magnitude higher than those required for the carbon replica opal samples (B/T ~ 0.7/38~1/50) presented here.

Dividing the right hand side of equation 1 by the quantum unit of resistance (h/e²) and the left hand side by B(1), the value of the magnetic field at the SdHass minimum associated with the unit hall resistance step then we obtain:

$$\frac{B}{B(1)} = \frac{R_{xy}(\Omega)}{(h/e^2)}$$

or in these normalized units of field (B_{norm}) and resistance (R*),

$$B_{norm} = R^* \quad \dots 4$$

Equation 4 predicts that any set of QHE data when plotted in the variables B_{norm} and R*, follow a direct universal direct proportionality with unit slope. This proportionality holds irrespective of the (positive or negative) sign of the carrier or their density and independent of the sample temperature. To test this proportionality we normalized the R_{xy} and B data of figure 3 by dividing with 25812.4 Ω and 1.44 T respectively. Also for the purposes of comparison we digitized some QHE-literature values; such as, the data for v equal to 2,3,4,6 & 8 states in a crystal of Bi_{2-x}Sn_xTe₃²²; and for the 14,16,18, 20 & 22 states²⁴ in a sample comprising of lateral superlattices. Figure 4 provides a graphical demonstration of the universal unit proportionality of all the B_{norm} and R* quantum hall effect in these systems ²⁵⁻²⁷ including those of figure 3.

Quantum hall effect is a proof of charge carrier condensation in two-dimensional (2D) states. The sheet density (n_s) of the carrier in QHE systems vary considerably, in typical heterostructure ^{3,4,21} n_s is $\sim 10^{15}$ m⁻². For our system, we determine $n_s = 2.2 \times 10^{14}$ m⁻² from the slope of the B vs R_{xy} plot (equation 1). So these carbon replica opals are a low carrier density 2DEG system comparable to that of reference 26.

In bulk systems QHE is possible ^{23,27-30}. For example, Belenkii has reported integer effects in the defect states of layered bulk semiconductors such as InSe. Quantization steps associated with field induced spin-density-waves were reported in the Bechgaard salt (TMTSF)₂PF₆ and Kul'bachinskii observed integer QHE in Bi₂Te₂₃, Sb₂Te₂₃ and Bi_{2-x}Sb_xTe₃.

Carbon replica opal is a material with a rich variety of the low-dimensional features and an enormously large ratio of surface to volume. It is possible that in the carbon system, the QHE arise from 2-d, interface or surface states. Surface states are important for the condensation of QHE. Furthermore, in a bulk material low dimensional states can play a role²⁹ similar to the Anderson localized states for standard two-dimensional quantum hall systems. A central feature of the many-body, wave function that describes fractional quantum hall effect ^{3,4} is nodes. Having deep nodes in the wave function is one of the prime requirements of the Laughlin theory³⁰. The holes or “anti dots” in the carbon matrix keep the carriers away from these void regions forcing nodes to form in their wave function. The three-dimensional, multiply connected, topology can provide many pathways to amplify quantum interference. Transformation of compressible and incompressible quantum fluids forming dots and anti-dots are important³¹ in quantum hall systems.

In the carbon system, there are also self-similarity and geometric hierarchies such as “hole inside a hole”. The importance of hierarchies in QHE has been a focus of current research attention³²⁻³⁴. Transport coefficients can be greatly affected by geometric effects. For example, in narrow gap, inhomogeneous semiconductors this effect may be so strong that SdHaas signals are detectable even at room temperature¹⁰. The combination of a plethora of geometric features and low carrier density may be favorable for the formation of quantum-hall condensates in the low B/T limit.

To the best of our knowledge, the current work is the first observation of quantum hall signals at temperatures well above the boiling point of liquid helium and in the very soft quantum limit. It is possible that QHE may occur at even higher temperatures. High temperatures will render these effects more accessible and may enable widespread technological applications.

Acknowledgements:

We wish to acknowledge Dr. Ray Baughmann for providing the specimens of carbon replica opal, Dr. Eric Palm for assistance with the high β facility at the NHMFL. The USC NanoCenter and the Materials Science and Technology Division of the Naval Research Laboratory provided partial supports to the first author.

References & foot notes:

§ Mathematically equations 2 is equivalent to the following equation:

$$(B)^{-1} = \left(\frac{e}{n_s h}\right) v \quad (2b)$$

But one may be preferable over the other. Typically, the form that distributes the ordinates and abscissas of the data points more evenly is chosen.

1. von Klitzing, K., Dorda, G. and Pepper, M. New Method of High- Accuracy Determination of the Fine-Structure Constant Based on Quantized Hall Resistance, *PRL*, **45**, 494 (1980)
2. Tsui, D.C., Stormer, H.L. and Gossard, A.C. Two-Dimensional Magnetotransport in the Extreme Quantum Limit, *Phys. Rev. Lett.* **48**, 1559 (1982)
3. *The Quantum Hall Effects Integral and Fractional*, 2nd edition by T. Chakraborty and Pekka Pietilainen, Springer-Verlag, Heidelberg (1995)
4. *The Quantum Hall Effect* edited by Richard E. Prange and Steven M. Girvin, Springer-Verlag, Heidelberg (1987)
5. Van Degrift, C.T., et al, Re-examination of Quantum Hall Plateaus, *IEE Transactions on Inst. & measurements*, **42**, 562, (1993)
6. Mani, R.G and von Klitzing K. Temperature-insensitive offset reduction in a Hall effect device, *Appl. Phys. Lett.* **64**, 3121 (1994)
7. W.Knap et al, Cyclotron resonance and quantum hall effect studies of the two dimensional electron gas confined at the GaN/AlGaN interface, *Appl. Phys. Lett.* **70**, 2123 (1997)
8. E. Frayssinet et al, High electron mobility in AlGaN/GaN heterostructures grown on bulk GaN substrates, *Appl. Phys. Lett.* **77**, 2551(2000)
9. Huckestein, B. Quantum Hall Effect at Low Magnetic Fields, *Phys. Rev. Lett.* **84**, 3141 (2000)
10. Solin, S. A., et al, Enhanced Room-Temperature Geometric Magnetoresistance in Inhomogeneous Narrow-Gap Semiconductors, *Science* **289**, 1530 (2000)
11. Kroemer,H. Polar-on-non-polar epitaxy, *J.Cryst.Growth* **81**, 193 (1987)
12. Wang,T., Moll,N., Cho,K., Joannopoulos, J.D. Deliberately designed materials for optoelectronics applications. *Phys. Rev. Lett.* **82**,3304 (1999)
13. Braff, G.A., Appelbaum,J.A., Hamann,D.R. Self-consistant calculation of electronic structure at an abrupt GaAs-Ge interface. *Phys. Rev. Lett.* **38**, 237 (1977)

14. Ohtomo,A., Hwang, H.Y. A high-mobility electron gas at the LaAlO₃-SrTiO₃ heterointerface. *Nature*, **427**, 423 (2004)
15. Bogomolov, V.; Kumzerov, Y.; and Romanov, S. Fabrication of Three-Dimensional Superlattice of Nanostructures , in *Physics of Nanostructures*, edited by Davies, J.H. and Long, A.R. Inst. Of Physics, Bristol and Philadelphia (1992) and references therein.
16. Zakhidov,A.A. et al, Carbon Structures with Three-Dimensional Periodicity at Optical Wavelengths, *Science*, **282**, 897 (1998).
17. Vlasov, Y.A., et al, On-chip natural assembly of silicon photonic bandgap crystals, *Nature*, **414**, 289 (2001).
18. Lungu, Anca et al, Superconductivity in Nanostructured Lead, *Physica C*, **349**, 1 (2001).
19. Bleiweiss, M. C., Magnetic and Transport Properties of Nanostructured Materials and Other Novel Systems, Ph.D., Dissertation, USC, (2001)
20. Kajii, H.,et al, Optical and electrical properties of opal carbon replica and effects of pyrolysis, *Jr. Of Appl. Phys.*, **88**, 758, (2000).
21. Datta, T., Yin, Ming and Bleiweiss, M, Universal Direct Proportionality: A New Analysis of Quantum Hall Effect. Preprint-<http://arxiv.org/cond-mat/0312687> and references therein.
22. Pan, W., et al, Fractional Quantum Hall Effect of Composite Fermions, *Phys. Rev. Let*, **90**, 016801 (2003).
23. Kul'bachinskii, V.A., et al. Quantum Hall Effect in the Bulk Semiconductors Bismuth and Antimony Tellurides: Proof of the Existence of a Current Carrier Reservoir, *JETP Let*, **70**, 767 (1999).Digitized data from figure 2, page 769.
24. Albrecht, C., et al, Evidence of Hofstadter's Fractal Energy Spectrum in the Quantum Hall Conductance, *Phys. Rev. Let*, **86**, 147 (2001). Digitized data from figure 2, page 149.
25. Digitized data from figure 4.2 in reference 3, page 34.
26. Belenkii, G.L., Electron-hole liquid and two-dimensional electron gas in layered group A³B⁶ semiconductors, *Sov. Phys. Usp*, **31**, 955 (1988)

27. Chamberlin, R.V., et al, Extreme Quantum Limit in a Quasi Two-Dimensional Organic Conductor, *Phys. Rev. Let.*, **60**, 1189 (1988)
28. Hannahs, S.T., et al, Quantum Hall Effect in a Bulk Crystal, *Phys. Rev. Let.*, **63**, 1988 (1989)
29. Hill, S. et al, Bulk quantum Hall effect: Evidence that surface states play a key role, *Phys. Rev. B*, **55**, R4891 (1997)
30. Laughlin, R.B., Anomalous Quantum Hall Effect: An Incompressible Quantum Fluid with Fractionally Charged Excitations, *Phys. Rev. Let.*, **50**, 1395 (1983)
31. Ilani, S., et al, The microscopic nature of localization in the quantum hall effect, *Nature*, 427, 328(2004)
32. Kane, C.L., Mukhopadhyay, R., Lubensky, L.C., Fractional Quantum Hall Effect in an array of Quantum Wires, *Phys. Rev. Let.*, **88**, 036401 (2002)
33. Mani, R.G., von Klitzing, K., Fractional quantum Hall effects as an example of fractal geometry of nature *Z.Phys. B*, **100**, 635 (1996)
34. Jurgen H. S. Quantum physics: Wheels within wheels, *Nature*, **422**, 391 (2003)

Figures:

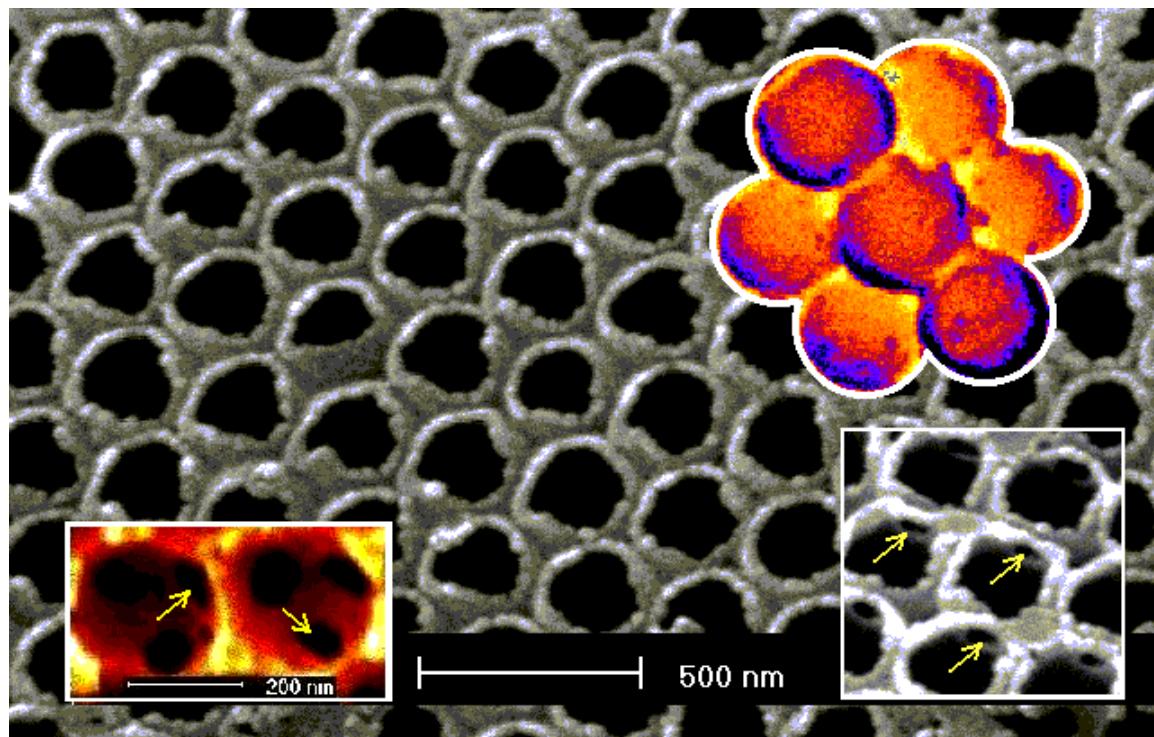


Figure-1: Electron micrograph of a QHE active, carbon replica opal (CRO) sample. The packing of the chemical vapor deposited carbon regions is shown. To show how the original opal underlies the replica structure, a color rendered image of the basic building block, a cluster of silica spheres is superposed on the top right hand corner. The insets at the bottom show details of the holes in the carbon. The size scales of the whole picture and that of the small inset are indicated.

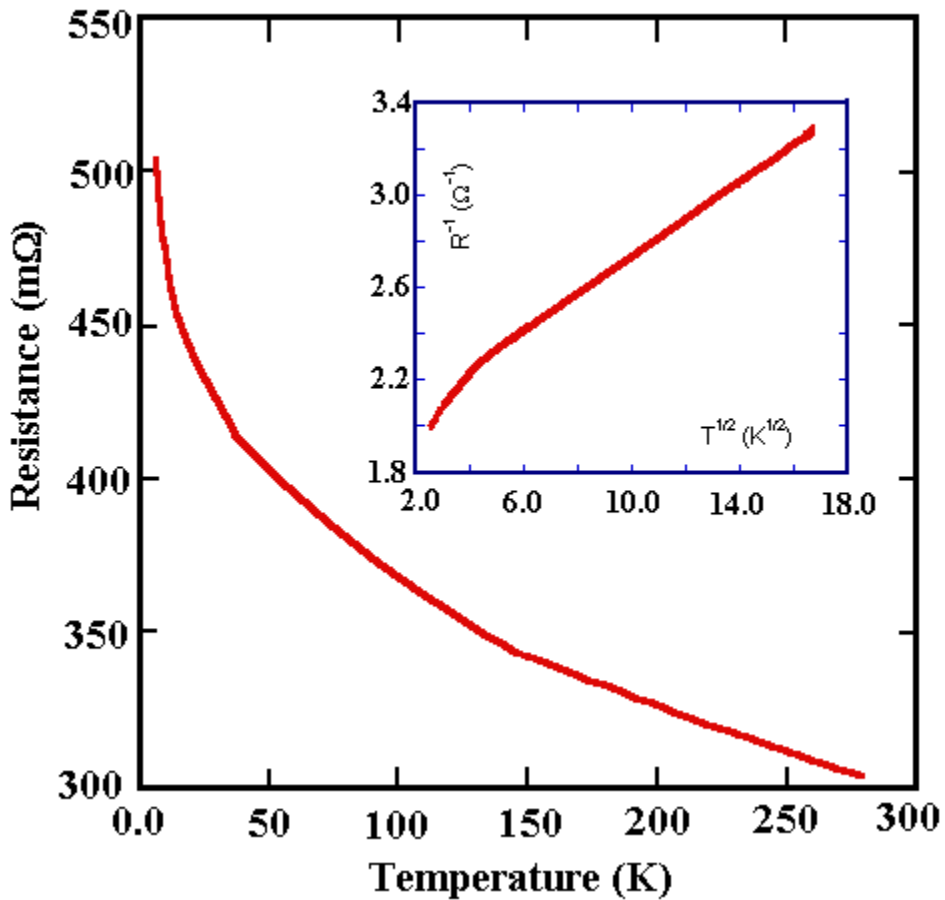


Figure-2: Electrical resistance of a carbon replica opal as a function of temperature. As may be seen the behavior is non metallic that is resistance increases as temperature decreases. Furthermore at low temperatures hopping conduction and weak localization are indicated as shown by the inset plot.

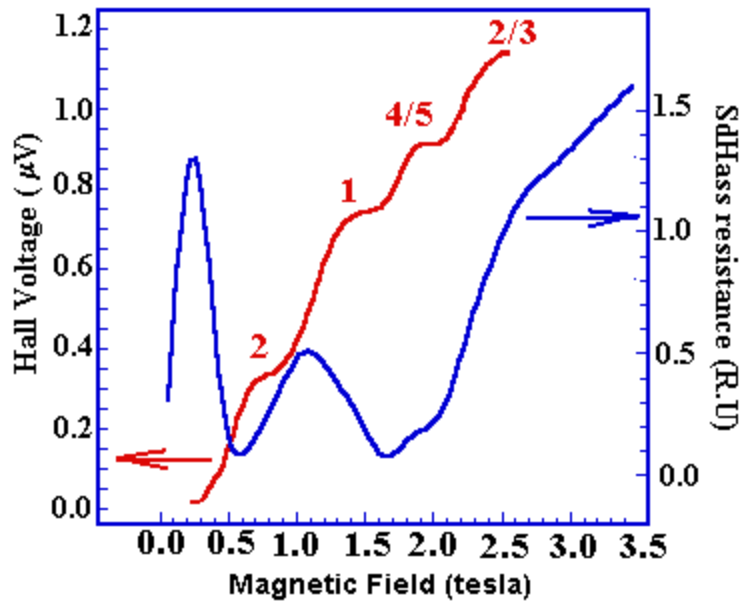


Figure-3: A von Klitzing plot at a temperature of 38 K shows the Shubnikov-deHaas oscillations (blue curve) and associated hall plateaus (red curve). The values of the filling factors estimated from equation 2 are also indicated. The arrows point the respective scales appropriate for each of the curves.

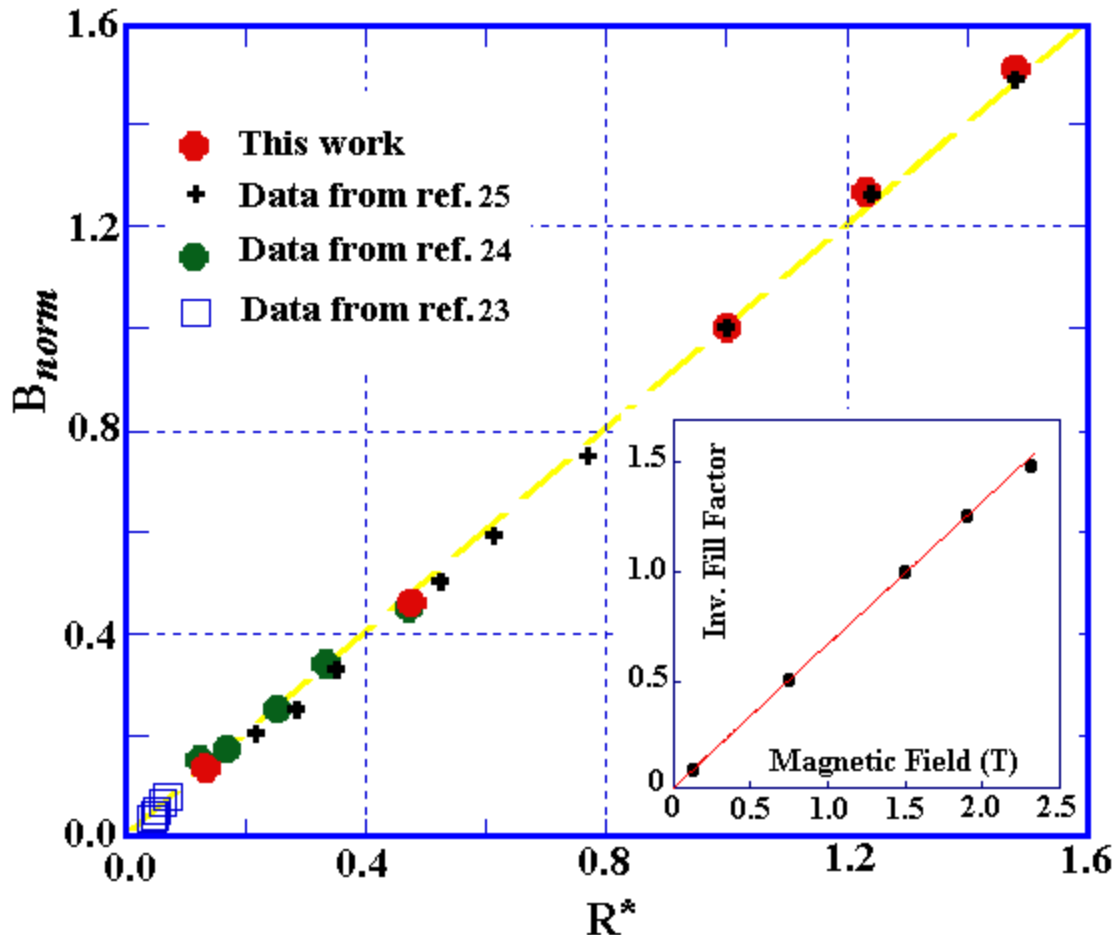


Figure-4: Universal proportionality of B_{norm} (the magnetic field B normalized by the field at unit step) versus R^* , the value of resistance (in units of h/e^2) and comparison of quantum Hall effect data from this work and three other sources in the published literature²⁴⁻²⁷. The inset shows the fit of equation 2 used for the determination of the fill factor (ν) values indicated in figure 3.